

STACKING ORANGES: A STUDY OF SQUARE ICE ANALOGUES OF PLANE PARTITIONS

A Project Report

submitted by

VARSHA SUBRAMANYAN

*in partial fulfilment of the requirements
for the award of the degree of*

BACHELOR OF TECHNOLOGY

&

MASTER OF TECHNOLOGY



**DEPARTMENT OF ELECTRICAL ENGINEERING
INDIAN INSTITUTE OF TECHNOLOGY MADRAS.**

MAY 2016

THESIS CERTIFICATE

This is to certify that the thesis titled **STACKING ORANGES: A STUDY OF SQUARE ICE ANALOGUES OF PLANE PARTITIONS**, submitted by **Varsha Subramanyan**, to the Indian Institute of Technology, Madras, for the award of the degree of **Bachelor of Technology** and **Master of Technology**, is a bona fide record of the research work done by her under our supervision. The contents of this thesis, in full or in parts, have not been submitted to any other Institute or University for the award of any degree or diploma.

Prof.Suresh Govindarajan

Research Guide

Professor

Dept. of Physics

IIT-Madras, 600 036

Place: Chennai

Prof.Nandita Dasgupta

Co-Guide

Professor

Dept. of Electrical Engineering

IIT-Madras, 600 036

Date: 1st May 2016

ACKNOWLEDGEMENTS

I would like to express my immense gratitude towards Prof. Suresh Govindarajan for being a mentor and guide to me over the last two years. Working with him was an opportunity to understand the workings of research, to imbibe patience and persistence, and to learn from my mistakes. He was a constant source of support and encouragement when I decided to transition to studying Physics. I would like to thank him for being an inspiration to me, both inside and outside the classroom.

I would like to thank Prof.Nicolas Destainville, whose earlier simulations were extremely crucial in the development of this thesis.

I would also like to thank Prof.V.Balakrishnan, Prof.Arul Lakshminarayan and Prof.Dawood Kothawala whose classes were powerful impetuses in driving me towards pursuing Physics. I also thank Prof.Nandita Dasgupta for being my co-guide.

Finally, I would like to thank Nirupama Jayaraman, Nithin Sivadas, Sabarish Reddy and other friends, for all their emotional support and companionship.

ABSTRACT

KEYWORDS: Square Ice, Plane Partitions

The square ice is a model in statistical physics describing certain configurations of water molecules on a 2D lattice. The model can be fully solved under certain boundary conditions, but this is not always possible. Therefore, we attempt an enumeration of these configurations. In order to do so square ice is recast as an analogue of plane partitions. Hence, it's enumeration may be studied as a problem in combinatorics and solved by numerical methods.

In this thesis, we estimate the asymptotic behaviour of these configurations by counting the combinatorics equivalent. The bounds for the asymptotic behaviour are analytically determined, and then established by means of Monte Carlo simulations, with suitable error bars.

TABLE OF CONTENTS

ACKNOWLEDGEMENTS	i
ABSTRACT	ii
LIST OF TABLES	v
LIST OF FIGURES	1
1 INTRODUCTION	2
1.1 Introduction to Square Ice	2
1.2 Other related Combinatorics Problems	4
1.2.1 Alternating Sign Matrices	4
2 PARTITIONS	6
2.1 Definitions	6
2.2 Counting of Partitions	7
2.3 Young Diagrams	8
2.4 Plane Partitions	10
2.4.1 Pyramid Partitions	11
2.5 Plane Partitions and the Five Vertex model	13
2.5.1 Square ice analogues of plane partitions	14
3 Square Ice Analogues	16
3.1 Square Ice as Lattice Paths	16
3.2 Square Ice as Heights	16
3.3 The Generalized Square Ice	17
3.4 The Oranges Formulation	18
3.5 The Counting Problem	19
4 Analytical Results	21
4.1 2D Oranges	21

4.2	Some results on partitions	23
4.2.1	Addition and Deletion Operators	23
4.3	Analytic form of $a_\ell(n)$	25
4.3.1	Conjecture on generalized $a_\ell(n)$	28
4.4	Analytic bounds on $a_\ell(n)$	28
4.4.1	Lower Bound for $a_\ell(n)$	29
4.4.2	Upper Bound on $a_\ell(n)$	30
4.4.3	Final conjecture	30
5	Simulation Methods	32
5.1	Monte Carlo simulations	32
5.1.1	The Metropolis-Hastings Algorithm	32
5.2	Transition Matrix Monte Carlo	33
6	Results	37
6.1	Results of the simulation	37
6.2	Summary of results	39
7	Conclusion and Unresolved Issues	44
A	The Bratley-McKay Algorithm	45

LIST OF TABLES

2.1	Explicit enumeration of partitions for dimensions from 1 to 5. These sequences can be found on [1]	12
3.1	Height function h_0 for $\ell = 1, 2, 3$	17
4.1	Explicit enumeration of $a_\ell(n)$ for $\ell = 1, \dots, 6$	26
6.1	Results of the three parameter fit.	38
6.2	Results of the four parameter fit.	38
6.3	Results of the two parameter fit.	38
6.4	Fit to analytic form to estimate A_ℓ	39
6.5	Data for $n_+(n)$, evaluated exactly by the Bratley-McKay algorithm.	40
6.6	Data for $n_-(n)$, evaluated exactly by the Bratley-McKay algorithm.	41

LIST OF FIGURES

1.1	The allowed vertices of the six vertex model, with associated weights.	3
1.2	Boundary conditions on Square Ice - the configuration on top has the open boundary condition imposed on it, while the second configuration has the domain wall boundary condition imposed on it.	3
1.3	A square ice configuration and the corresponding alternating sign matrix it maps on to.	5
2.1	The Young Lattice for integer partitions in terms of Young diagrams, explained in Section 2.3 (Source: David Eppstein, Wikimedia Commons)	7
2.2	A plane partition of 32 in the isometric view.	10
2.3	Young diagram representation of the plane partition in Figure 2.2.	10
2.4	The plane partitions of 4.	11
2.5	An empty pyramid partition, with 3 blocks on top.	12
2.6	Example configuration to be converted to lattice paths.	14
2.7	The allowed vertices of the five vertex model, with the transformations required to map onto lattice paths.	14
2.8	Lattice paths on the five vertex configuration.	15
2.9	Lattice paths converted to a plane partition.	15
3.1	Map for conversion of the six vertex model to lattice paths.	16
3.2	Map for conversion of the six vertex model to heights. [2]	16
3.3	A stack of oranges with $\ell = 1$, with no oranges removed.	19
3.4	A stack of oranges with $\ell = 3$, with no oranges removed.	19
3.5	A square ice configuration of $\ell = 1$ decomposed into 4 plane partitions	20
3.6	A square ice configuration of $\ell = 4$ decomposed into 4 plane partitions, except for the missing piece in white, which is negligible for $\ell \ll n^{1/3}$.	20
4.1	A stack of 2D oranges with $\ell = 1$	21
4.2	The red oranges represent the oranges that have been removed from the stack. Counting the number of ways of removing oranges from such a stack is clearly given by integer partitions, as can be seen from the second figure.	22

4.3	A stack of $\ell = 3$ with the corresponding partition representation. The blue part represents the missing portion, which results in the counting being given by shifted partitions.	22
4.4	Here, the blue nodes belong to $S_+(\lambda)$ and the green nodes belong to $S_-(\lambda)$	23
4.5	Plots for $n_+(n)$, $n_-(n)$ and their difference, for integer partitions(top) and plane partitions(bottom). The averages data (in blue) have been fit to the model described in Proposition 3. The fit for n_+ is in green and the fit for n_- is in red. The difference plot shows the leading behaviour is $n^{d-1/d+1}$, which in the case of integer partitions is a constant, viz. 1.	25
4.6	An example of a configuration with no removable one-part.	28
4.7	An example of a configuration with a removable one-part.	28
4.8	A configuration of $\ell = 4$ and $n = 46$	29
6.1	Plots of $\log \frac{a_\ell(n-1)}{a_\ell(n)}$ versus $n^{-1/3}$. The three fits, along with actual data and simulation data. The green points indicate explicitly enumerated data, the red points are the data generated in simulation. The pink line is the three parameter fit, the brown line is the three parameter fit, and the blue line is the four parameter fit. Note that they all agree for $n^{-1/3} \ll \ell^{-1}$. The plots represent data from $\ell = 1, \dots, 6$. Key: Black plot - Two parameter fit, Blue plot - Three parameter fit, Purple plot - Four parameter fit, Red points - Simulated data, Green points - Actual data	42
6.2	A fit of g as a function of ℓ	42
6.3	A fit of $\log A_\ell$ as a function of ℓ	43

CHAPTER 1

INTRODUCTION

1.1 Introduction to Square Ice

A vertex model is a model in statistical mechanics where boltzmann weights are assigned to each of a set of possible vertices associated with the model. The particles being described by these models live on the vertices, and the interactions are described by the type of vertex, rather than by bonds with adjacent particles, like the Ising model.

An ice-type model is a type of vertex model where each vertex represents a water molecule. The vertices are connected by directed edges. They are called "square ice" when represented on a 2D lattice, with coordination number 4. Ice type models were originally proposed by Linus Pauling [3] to calculate the residual entropy of water ice, giving the model its name. In 1967, Elliot Lieb found the exact solution to the residual entropy problem for 2D square ice. The residual entropy was expressed as $S = NK_B \log W$, where W was calculated as $(\frac{4}{3})^{3/2}$. This is known as Lieb's square ice constant [4].

Each configuration of square ice represents an arrangement of water molecules on a plane, with the constraint that every vertex represents an oxygen atom, and is surrounded by four hydrogen atoms. Since the oxygen atom can only be attached to two hydrogens out of four, the hydrogen atoms attached to the oxygen are represented by edges pointing towards it, and those unattached are represented by edges pointing away from it. It is clear that there are six such lattice point configurations of the water molecule. Hence, square ice is also called the six-vertex model. Generalizations of the model can be constructed in terms of the eight, or sixteen vertex models. Figure 1.1 shows the six possible vertex configurations.

Solving square ice is dependent on the boundary conditions imposed on it. The open boundary condition, with vertical boundaries having arrows pointing outwards, and horizontal boundaries having arrows pointing inwards could be imposed, or the domain

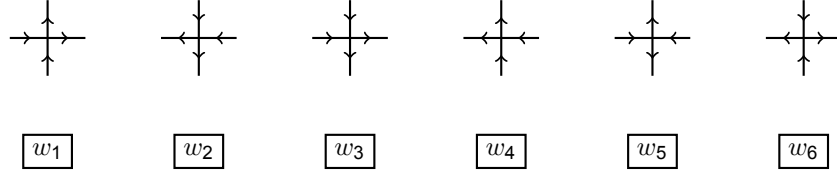


Figure 1.1: The allowed vertices of the six vertex model, with associated weights.

wall boundary conditions, as represented below, are some possible boundary conditions.

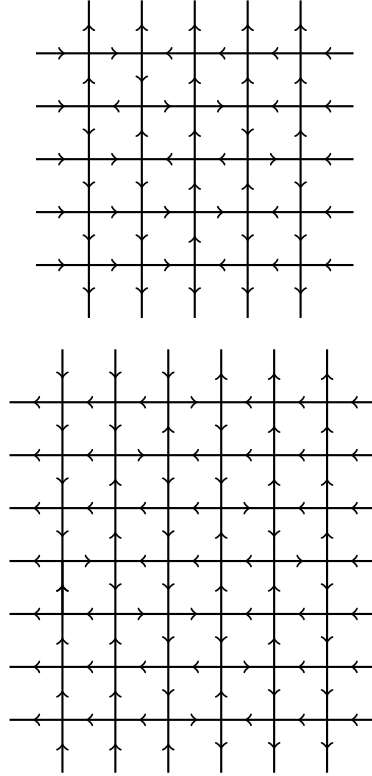


Figure 1.2: Boundary conditions on Square Ice - the configuration on top has the open boundary condition imposed on it, while the second configuration has the domain wall boundary condition imposed on it.

A partition function can be written for the model by assigning energies ϵ_i , and hence boltzmann weights, to each of the 6 vertex types, as follows -

$$Z = \sum_{\{n_i\}} e^{-\frac{\epsilon}{k_B T}}, \text{ where } \epsilon = \sum_{i=1}^6 n_i \epsilon_i. \quad (1.1)$$

This sum can be written to account for various boundary conditions, or to accommodate constraints in the energy levels, leading to sub-classes of the square ice model. Solving the model completely involves determination of the partition function, or equivalently, counting all possible configurations on the lattice. While it is possible to exactly solve

the six vertex model under specific boundary conditions, it might not be possible to obtain closed form solutions for others. In cases where closed form solutions cannot be obtained, we adopt other methods to study the model, one of which is described in this project.

1.2 Other related Combinatorics Problems

The square ice model can be bijectively mapped onto various other combinatorial problems, like Alternating Sign Matrices, Domino Tilings etc. These maps aid in understanding both objects better, and have lead to seminal discoveries. One of the proofs of the ASM conjecture was given by Zeilberger using the square ice model [5]. The map from square ice to alternating sign matrices is described below.

1.2.1 Alternating Sign Matrices

An alternating sign matrix (ASM) is an $n \times n$ square matrix which obeys the following constraints -

- The matrix is composed of only $-1, 0$ and 1
- The non-zero entries in each row and column alternate in sign
- The sum of entries in each row and each column is 1

Every configuration of the six vertex model can be bijectively mapped onto an alternating sign matrix.

Consider an $n \times n$ patch of square ice, with boundary conditions such that the vertical arrows on the boundary point outwards, and the horizontal arrows on the boundary point inwards. Each vertex has 2 incoming arrows. Replace every vertex that has both incoming arrows on the horizontal with $+1$, and every vertex with both incoming arrows on the vertical with -1 . Every other vertex is replaced by 0 . This gives an $n \times n$ ASM. The map is reversible in every step, and hence, forms a bijection [6]. Figure 1.3 shows a configuration of square ice with domain wall boundary conditions, and the corresponding ASM that it maps on to.

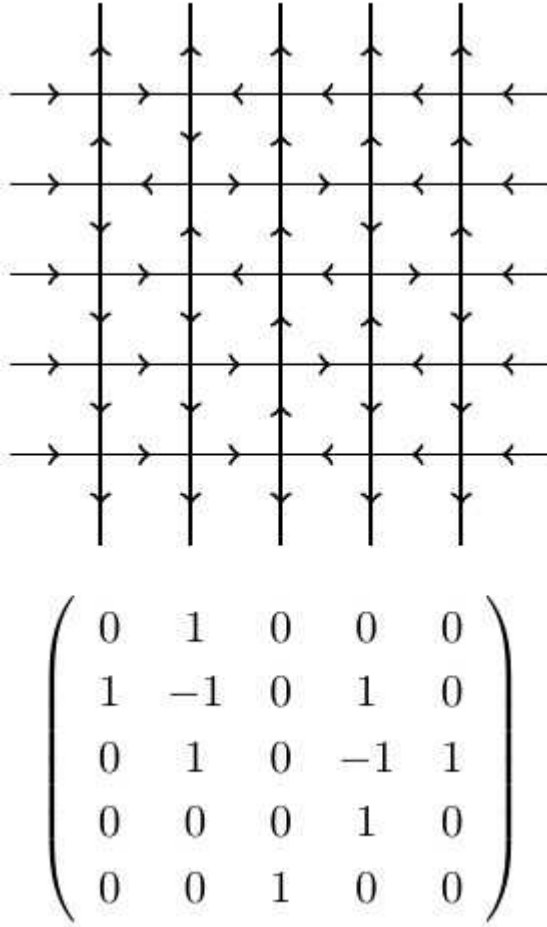


Figure 1.3: A square ice configuration and the corresponding alternating sign matrix it maps on to.

It is also interesting to note that ASMs have the same enumeration as totally symmetric self-complementary plane partitions (TSSCPPs). A totally symmetric plane partition of size n is a plane partition whose Young diagram is contained in a box of size $n \times n \times n$ and which is mapped to itself under all permutations of the coordinate axes. A totally symmetric plane partition is self-complementary if it is identical to its complement within the same box. The TSSCPP conjecture was first proposed by G. Andrews [7]. Zeilberger later showed that they are equinumerous with ASMs, though his proof was not bijective. A bijection between the two objects is yet to be established.

This thesis is an attempt to study the asymptotic behaviour of configurations of the generalized square ice model, by casting it as an analogue of plane partitions, and using properties of plane partitions to solve it as a problem in combinatorics.

CHAPTER 2

PARTITIONS

2.1 Definitions

A **partition** of a positive integer n is a representation of n as a sum of positive integers lesser than itself. Formally,

Definition 2.1. *The set $\lambda = \{S_i\}$ is a partition of n if $\sum_i S_i = n$, $S_i \in \mathbb{N}$.*

It is denoted by $\lambda \vdash n$. Each S_i is called a **part** of the partition λ . Partitions are order independent, i.e., sums that differ only by the order of their summands are considered to be the same partition. For example: The positive integer 5 has the following 7 distinct partitions -

$$(5), (4 + 1), (3 + 2), (3 + 1 + 1), (2 + 2 + 1), (2 + 1 + 1 + 1), (1 + 1 + 1 + 1 + 1).$$

Partitions are usually represented by means of Young diagrams, or Ferrer diagrams. The growth of partitions along integers can be represented by means of a Young lattice. Traversing any arm of the Young Lattice results in a unique partition. Mathematically, a lattice is defined as a partially ordered set in which every two elements of the set consist of a unique supremum and a unique infimum. It is clear that Young lattice follows this definition.

Young diagrams are a special case of Bratteli diagrams, which are defined in the following way [8].

Definition 2.2. *A Bratteli diagram is an oriented graph $\Gamma = \bigcup_{n \geq 0} \Gamma_i$, where each Γ_i is a set of vertices at level i . It has the following properties -*

- Γ_0 is the vertex ϕ .
- If an edge starts at a vertex in Γ_i , then it ends at a vertex in Γ_{i+1} .
- Every vertex has at least one outgoing edge.
- All Γ_i are finite sets.

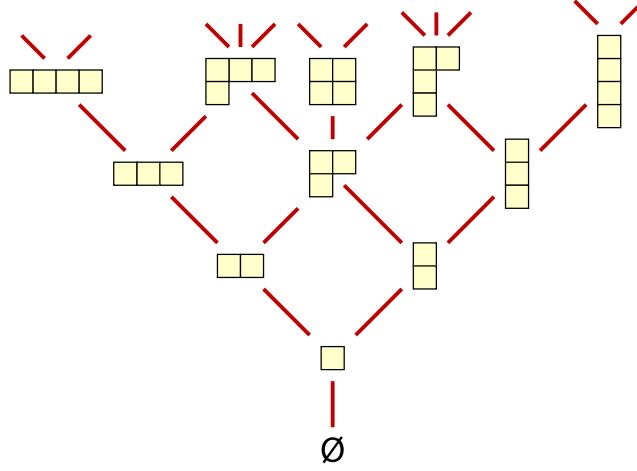


Figure 2.1: The Young Lattice for integer partitions in terms of Young diagrams, explained in Section 2.3 (Source: David Eppstein, Wikimedia Commons)

Partitions have rich structure and well-documented properties in number theory and combinatorics. They find applications in a number of areas in Physics and Mathematics, like the representation theory of symmetric groups.

2.2 Counting of Partitions

We define a generating function for integer partitions, of the form $F(q) = \sum_{i=0}^{\infty} a_i q^i$, where a_i denotes the number of partitions of i .

Theorem 2.1. *The generating function for integer partitions is given by*

$$F(q) = \prod_{i=1}^{\infty} (1 - q^i)^{-1}.$$

Proof. Consider

$$F_1(q) = \frac{1}{1 - q} = 1 + q + q^2 + q^3 + \dots = \sum_{i=0}^{\infty} a_i^{(1)} q^i,$$

$$F_2(q) = \frac{1}{(1 - q)(1 - q^2)} = (1 + q + q^2 + q^3 + \dots)(1 + q^2 + q^4 + q^6 + \dots) = \sum_{i=0}^{\infty} a_i^{(2)} q^i.$$

Clearly, the coefficient of q^n in $F_1(q)$, $a_n^{(1)}$ gives the number of ways in which n , the power of q , can be enumerated as a sum of 1s viz. 1. Correspondingly, the coefficient of q^n in $F_2(q)$, $a_n^{(2)}$ gives the number of ways of expressing n as a sum of 1s and 2s.

Therefore,

$$F_m(q) = \prod_{i=1}^m (1 - q^i)^{-1} = \sum_{i=0}^{\infty} a_i^{(m)} q^i$$

gives coefficients $a_i^{(m)}$ that express n as a sum of integers lesser than or equal to m . By extension, the generating function for integer partitions is given by

$$F(q) = \sum_{i=0}^{\infty} a_i q^i = \prod_{i=1}^{\infty} (1 - q^i)^{-1}.$$

□

Enumerating the function gives the following sequence -

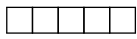
1, 1, 2, 3, 5, 7, 11, 15, 22, 30, 42, 56, 77, 101, 135, 176, 231, 297, 385,...

This is the sequence of integer partitions.

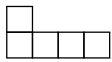
2.3 Young Diagrams

Partitions may be visually represented by means of **Young diagrams** or equivalently, **Ferrer Diagrams**. It consists of rows of boxes on a 2D plane. When the elements of S_i are decreasingly ordered, then a each element in the set denotes the number of boxes in the subsequent row.

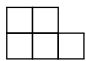
The following set of Young diagrams are drawn corresponding to the partitions of 5 -

1. 

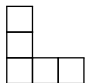
$$S_1 = \{5\}$$

2. 

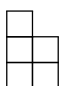
$$S_2 = \{1, 4\}$$

3. 

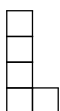
$$S_3 = \{2, 3\}$$

4. 

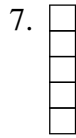
$$S_4 = \{1, 1, 3\}$$

5. 

$$S_5 = \{1, 2, 2\}$$

6. 

$$S_6 = \{1, 1, 1, 2\}$$



$$S_7 = \{1, 1, 1, 1, 1\}$$

When represented on the cartesian plane with origin at the bottom-left corner, each square of a Young diagram has an associated pair of co-ordinates. Thus, partitions can also be defined by means of these Young diagrams.

Definition 2.3. A partition λ of integer n can be defined as a collection of co-ordinates such that if $(x_1, y_1) \in \lambda$, then $(x_2, y_2) \in \lambda, \forall x_2 \leq x_1$ and $y_2 \leq y_1$. The total number of squares is n , and is also called the volume of the partition.

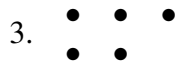
The two definitions are equivalent, and a unique diagram can be assigned to each partition, once a convention is chosen, as demonstrated by the example above. One could also draw Ferrer Diagrams, which are equivalent to Young diagrams.



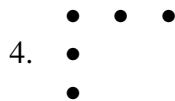
$$S_1 = \{5\}$$



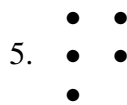
$$S_2 = \{4, 1\}$$



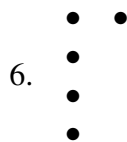
$$S_3 = \{3, 2\}$$



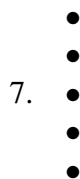
$$S_4 = \{3, 1, 1\}$$



$$S_5 = \{2, 2, 1\}$$



$$S_6 = \{2, 1, 1, 1\}$$



$$S_6 = \{1, 1, 1, 1, 1\}$$

2.4 Plane Partitions

Partitions, when expressed as a Young Diagram, with co-ordinates for each square, can easily be extended to higher dimensions - plane partitions in 2D and solid partitions in 3D.

Definition 2.4. A plane partition λ can be defined as a collection of co-ordinates such that if $(x_i, y_i, z_i) \in \lambda$, then $(x_j, y_j, z_j) \in \lambda, \forall x_j \leq x_i, y_j \leq y_i$ and $z_j \leq z_i$.

The following figure is one of the plane partitions of 26 -

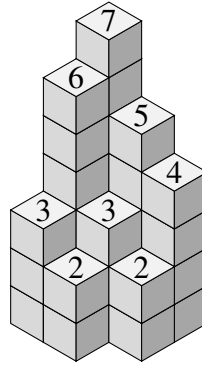


Figure 2.2: A plane partition of 32 in the isometric view.

One may also represent them in 2D, like a Young diagram, with numbers in each box denoting height of the plane partition in the dimension projecting out of the plane, as shown in Figure 2.3. The 13 plane partitions of 4 are drawn out in Figure 2.4.

4	2	
5	3	2
7	6	3

Figure 2.3: Young diagram representation of the plane partition in Figure 2.2.

The Young diagram definition of partitions could be extended to an arbitrary d dimensions. Therefore -

Definition 2.5. A d -dimensional partition λ of n can be defined as a collection of co-ordinates such that if $(x_i^{(1)}, x_i^{(2)}, \dots, x_i^{(d)}) \in \lambda$, then $(x_j^{(1)}, x_j^{(2)}, \dots, x_j^{(d)}) \in \lambda, \forall x_j^{(k)} \leq x_i^{(k)}, 1 \leq k \leq d$.

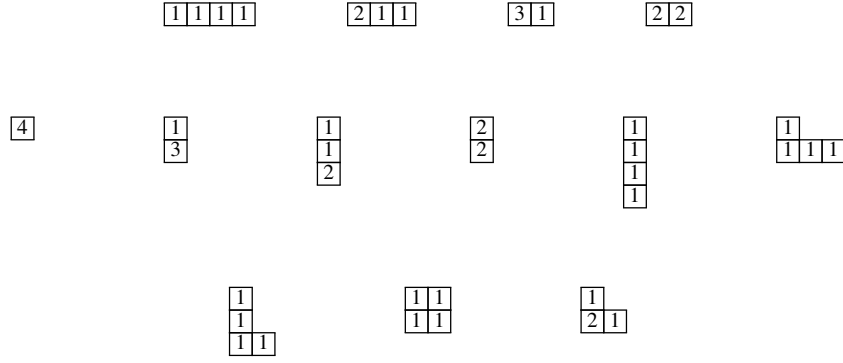


Figure 2.4: The plane partitions of 4.

Plane partitions are enumerated by the MacMahon function -

$$F(q) = \prod_{i=1}^{\infty} (1 - q^i)^{-i}.$$

While this may be seen as the 2D extension of the generating function for integer partitions, there is no analogous formula in 3D, for solid partitions. Further, the number of plane partitions that could fit into a box of dimensions $a \times b \times c$ is given by the MacMahon formula [9]-

$$M(a, b, c) = \prod_{i=1}^a \prod_{j=1}^b \prod_{k=1}^c \frac{i + j + k - 1}{i + j + k - 2}. \quad (2.1)$$

The formula was given by Percy MacMahon and later written in its current form by Ian MacDonald. Asymptotically, $\log(a_n) \sim n^{2/3}$, or $c_1 < n^{-2/3} \log(a_n) < c_2$, where c_1, c_2 are real constants. This form was worked out by E.M. Wright [10]. In general, one observes that a partition of d -dimensions assumes the following form asymptotically - $\log(a_n^d) \sim n^{d/d+1}$ [11].

The first few numbers for each dimension, generated via the Bratley-McKay algorithm (Appendix A) are given in Table 2.1.

2.4.1 Pyramid Partitions

Like square ice, pyramid partitions are also closely related to plane partitions. An empty pyramid partition, with n top layer blocks, and with no blocks removed is shown in Figure 2.5, and is denoted by ϵ_n .

$p_d(n) \backslash d$	1	2	3	4	5
$p(0)$	1	1	1	1	1
$p(1)$	1	1	1	1	1
$p(2)$	2	3	4	5	6
$p(3)$	3	6	10	15	21
$p(4)$	5	13	26	45	71
$p(5)$	7	24	59	120	216
$p(6)$	11	48	140	326	657
$p(7)$	15	86	307	835	1907
$p(8)$	22	160	684	2145	5507
$p(9)$	30	282	1464	5345	15522
$p(10)$	42	500	3122	13220	43352
$p(11)$	56	859	6500	32068	119140
$p(12)$	77	1479	13426	76965	323946
$p(13)$	101	2485	27248	181975	869476
$p(14)$	135	4167	54804	425490	2308071
$p(15)$	176	6879	108802	982615	6056581
$p(16)$	231	11297	214071	2245444	15724170
$p(17)$	297	18334	416849	5077090	40393693
$p(18)$	385	29601	805124	11371250	102736274
$p(19)$	490	47330	1541637	25235790	258790004
$p(20)$	627	75278	2930329	55536870	645968054
$p(21)$	792	118794	5528733	121250185	1598460229
$p(22)$	1002	186475	10362312	262769080	3923114261
$p(23)$	1255	290783	19295226	565502405	9554122089
$p(24)$	1575	451194	35713454	1209096875	23098084695
$p(25)$	1958	696033	65715094	2569270050	55458417125

Table 2.1: Explicit enumeration of partitions for dimensions from 1 to 5. These sequences can be found on [1]



Figure 2.5: An empty pyramid partition, with 3 blocks on top.

Definition 2.6. A pyramid partition of length n is a finite subset Π of the bricks of ϵ_n such that if B is a brick in Π , then all of the bricks of ϵ_n which rest upon B are also in Π [12].

The generating function for pyramid partitions can be expressed in closed form, and was first conjectured by Szendrői[13] (a special case of it by Kenyon), and was proved by Benjamin Young[12]. It is given by

$$Z^{(n)}(q_0, -q_1) = M(1, q_0 q_1)^2 \prod_{k \geq 1} (1 + q_0^k q_1^{k-1})^{k+n-1} \prod_{k \geq 1} (1 + q_0^k q_1^{k+1})^{\max(k-n+1, 0)}$$

where $M(x, q)$ is the MacMahon function

$$M(x, q) = \prod_{n=1}^{\infty} (1 - xq^n)^{-n}.$$

For $n = 1$, and when $q_0 = -qr$, $q_1 = -r^{-1}$, the generating function becomes that of a generalized version of plane partitions[13],

$$Z^{(1)} = M(1, q)^2 \prod_{k \geq 1} (1 + q^k r)^k \prod_{k \geq 1} (1 + q^k r^{-1})^k = M(1, q)^2 \prod_{k \geq 1} (1 - q^k r)^{-k} \prod_{k \geq 1} (1 - q^k r^{-1})^{-k}.$$

which can be written in the compact form

$$Z^{(1)} = M(1, q)^2 M(r, q) M(r^{-1}, q).$$

2.5 Plane Partitions and the Five Vertex model

A special case of the six vertex model is the five vertex model, where the weight w_1 is set to 0. Hence the vertex corresponding to this weight does not occur in any of the configurations. For finite sizes, under fixed boundary conditions, each configuration of square ice can be bijectively mapped onto a corresponding set of lattice paths, and hence onto row strict plane partitions [14].

Definition 2.7. A row strict plane partition is one in which the numbers in the boxes that denote height, strictly decrease along the rows of the partition.

Consider a configuration of vertices on a $2N \times (M + 1)$ lattice. The fixed boundary

conditions dictate that all arrows on the left and right boundaries point left, the arrows on the top and bottom boundaries of the first N columns point inwards, while the others point outwards. One such configuration is shown in Figure 2.6.

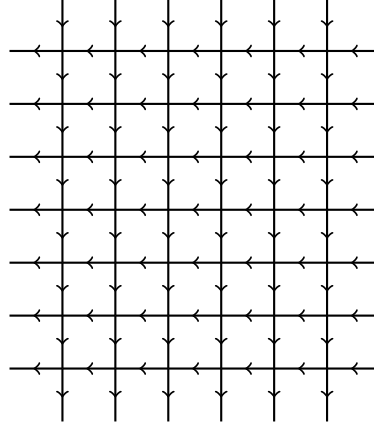


Figure 2.6: Example configuration to be converted to lattice paths.

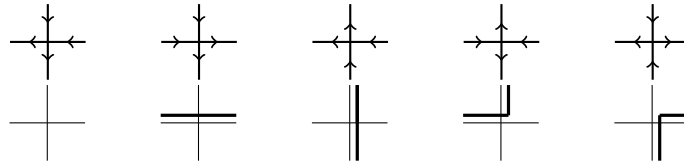


Figure 2.7: The allowed vertices of the five vertex model, with the transformations required to map onto lattice paths.

To describe the map, we associate each vertex with lines crossing the vertex, as shown in the Figure 2.7. Replacing each vertex by the lines results in lattice paths that begin in the south-west end of the lattice and travel towards the north-east. The associated row strict plane partition can be directly read off starting from the leftmost lattice path. Figures 2.8 and 2.9 show the lattice paths associated with the configuration in Figure 2.6, and the plane partition thus obtained. The bijection can be reversed step-wise to obtain a five-vertex configuration, given a row strict plane partition.

Counting the height at which each path makes each of its turns, gives the partition matrix, from which the partition is obtained.

2.5.1 Square ice analogues of plane partitions

The square ice model, when cast as a combinatorics problem, can be decomposed into four plane partitions, or skewed plane partitions. Hence, in the asymptotic limit, they behave similarly. This has been elaborated in Chapter 3.

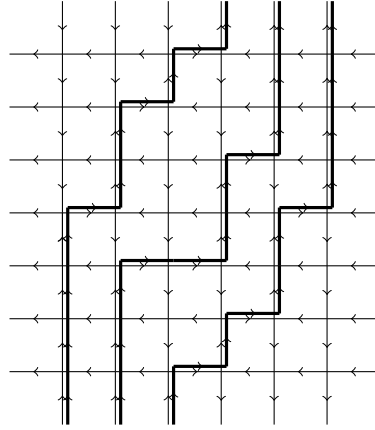
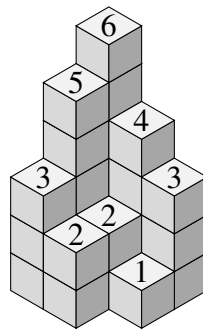


Figure 2.8: Lattice paths on the five vertex configuration.



$$\begin{pmatrix} 6 & 4 & 3 \\ 5 & 2 & 1 \\ 3 & 2 & 0 \end{pmatrix}$$

3	1	
4	2	2
6	5	3

Figure 2.9: Lattice paths converted to a plane partition.

CHAPTER 3

Square Ice Analogues

Square ice can be viewed in multiple ways, by defining maps on its structure. One such map for the finite lattice in the five vertex version has already been defined. Two other interpretations are described below.

3.1 Square Ice as Lattice Paths

The map from square ice to non-crossing lattice paths is an extension of the five-vertex map. It is obtained by replacing every configuration by the following lattice lines, leading to non-crossing paths. Since these are not further mapped onto row strict plane partitions, boundary conditions aren't defined for the map.

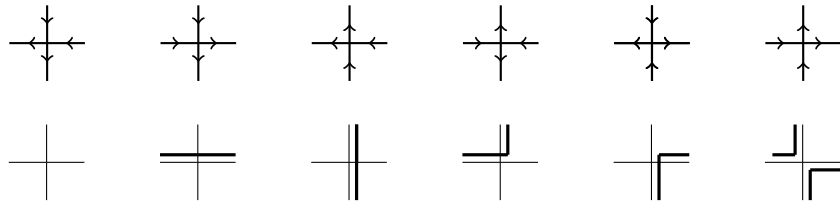


Figure 3.1: Map for conversion of the six vertex model to lattice paths.

3.2 Square Ice as Heights

It is also possible to associate a height function with the square ice configuration. This is obtained by associating the following map to every vertex of the lattice.

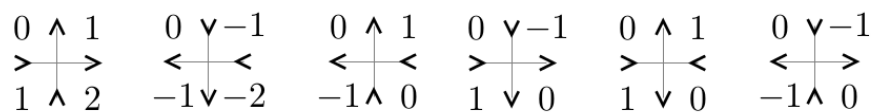


Figure 3.2: Map for conversion of the six vertex model to heights. [2]

Here, the numbers denote a change in height rather than absolute height. Hence it is clearly seen that the choice of origin is arbitrary as the difference in heights of any 2

points is independent of position of origin. This idea of height functions where neighbouring points differ in height by 1, can be generalized to define the model in a more precise manner.

3.3 The Generalized Square Ice

The generalized square ice model is described through the proposition of James Propp. Consider a 2D lattice \mathbb{Z}^2 , and define a height function h_0 on it, with parameter ℓ .

Definition 3.1. For every $v = (x, y) \in \mathbb{Z}^2$, define

$$h_0(v) = \begin{cases} |x| + |y| & x \in (-\infty, 0) \\ |x + y| & x \in [0, \ell) \\ |x - \ell + 1| + |y + \ell - 1| & x \in [\ell, \infty) \end{cases}$$

Clearly, ℓ describes the number of points with $h_0 = 0$.

4	3	2	3	4	4	3	2	3	4	2	1	2	3	4
3	2	1	2	3	3	2	1	2	3	1	0	1	2	3
2	1	0	1	2	2	1	0	1	2	2	1	0	1	2
3	2	1	2	3	3	2	1	0	1	3	2	1	0	1
4	3	2	3	4	4	3	2	1	2	4	3	2	1	2

Table 3.1: Height function h_0 for $\ell = 1, 2, 3$.

Also, define $h(u)$ on \mathbb{Z}^2 such that

- h agrees with h_0 on all but finitely many places on \mathbb{Z}^2 ,
- $h \geq h_0$,
- $|h(u) - h(v)| = 1$ for every adjacent u, v on \mathbb{Z}^2 .

Further, the reduced height function is defined as

$$r(u) = \frac{1}{2}(h(u) - h_0(u)). \quad (3.1)$$

The volume of the configuration is defined as $n = \sum r(u)$.

Proposition 3.1. The reduced height function r is such that, for u, v adjacent on \mathbb{Z}^2 , $|r(u) - r(v)| \in \{0, 1\}$.

Proof. Consider adjacent points u, v such that u is closer to the points on $x + y = 0$, $x \in [0, l)$, than v , with both points belonging in the $x \in (-\infty, 0)$ region.

$$r(u) - r(v) = \frac{1}{2}(h(u) - h(v)) - \frac{1}{2}(h_0(u) - h_0(v)),$$

$$h_0(u) - h_0(v) = |x_u| + |y_u| - |x_v| - |y_v|.$$

Since u and v are adjacent, they share one common co-ordinate and differ in the other by 1, and since u is closer to origin, $h_0(u) - h_0(v) = -1$. Similarly,

$$h_0(u) - h_0(v) = |x_u + y_u| - |x_v + y_v| = -1, x \in [0, l),$$

$$h_0(u) - h_0(v) = |x_u - \ell + 1| + |y_u + \ell - 1| - |x_v - \ell + 1| - |y_v + \ell - 1| = -1, x \in [\ell, \infty).$$

This follows in each case since the co-ordinates that differ by 1 are simply shifted by equal amounts. Now we consider the points along the lines of discontinuity -

$$h_0(u) - h_0(v) = |y| - |y| - 1 = -1 \text{ for } x_u = 0, x_v = -1,$$

$$h_0(u) - h_0(v) = |y + \ell - 1| - |\ell - \ell + 1| - |y + \ell - 1| = -1 \text{ for } x_u = \ell - 1, x_v = \ell.$$

By definition, for each case, $h(u) - h(v) \in \{-1, 1\}$. Therefore, it follows from the definition of the reduced height function that $r(u) - r(v) \in \{0, 1\}$. \square

This also shows that the $r(t, -t)$, $t \in [0, l)$ is the maximum of the reduced height function, and that it is weakly decreasing. Since volume is fixed, it can be seen that $r(x, y) = 0$ for $h_0(x, y) > n$ and the non-zero values lies within a square of length $2n$.

The problem is to count the number of such configurations of heights that can be obtained for each n , and determine this sequence $a_\ell(n)$ along with its generating function.

3.4 The Oranges Formulation

The question can be recast as a combinatorics problem (as proposed by R. Kenyon). Consider an infinite 3D prism of oranges, stacked such that the k -th layer of oranges from the top is a rectangle having $k \times (k + \ell - 1)$ spheres. Therefore, the prism has a peak of length ℓ , when $k = 1$. Figure 3.3 shows the stack of oranges in question. The number of ways to remove n spheres from the pyramid without disturbing the other

spheres gives the sequence $a_\ell(n)$. Every orange removed from the stack corresponds to an increase in the reduced height by 1, in the height function formulation. That is, an untouched stack corresponds to a configuration where the reduced heights is zero everywhere. As oranges are picked, the configuration builds up. Thus, the problem of counting the number of ways of unstacking oranges is equivalent to the height function interpretation of the generalized square ice.

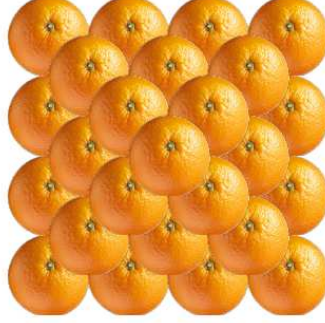


Figure 3.3: A stack of oranges with $\ell = 1$, with no oranges removed.

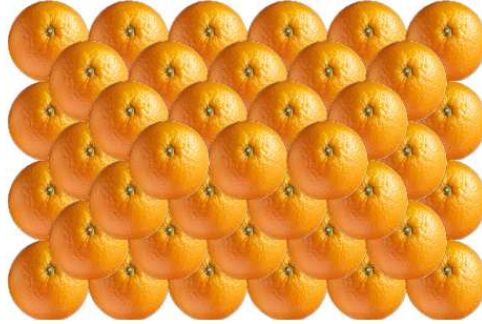


Figure 3.4: A stack of oranges with $\ell = 3$, with no oranges removed.

3.5 The Counting Problem

The sequence $a_\ell(n)$ does not have a closed form representation. But it is possible to determine the behaviour of $a_\ell(n)$ for a given ℓ . We can analytically determine the asymptotic behaviour by breaking the lattice, or stack of oranges, into 4 plane partitions each.

Decomposing the stack this way gives us an idea about the long range behaviour of $a_\ell(n)$. It is clear that the asymptotic behaviour would be similar to that of plane partitions. A detailed analysis of the asymptotics is done in a subsequent chapter.

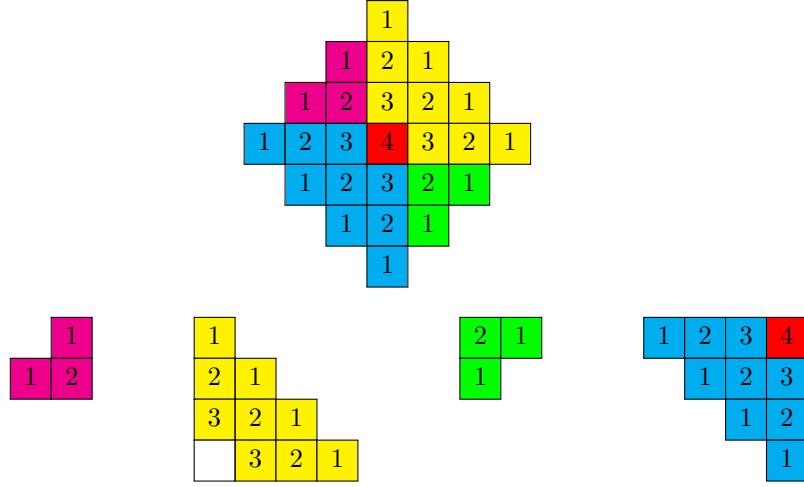


Figure 3.5: A square ice configuration of $\ell = 1$ decomposed into 4 plane partitions

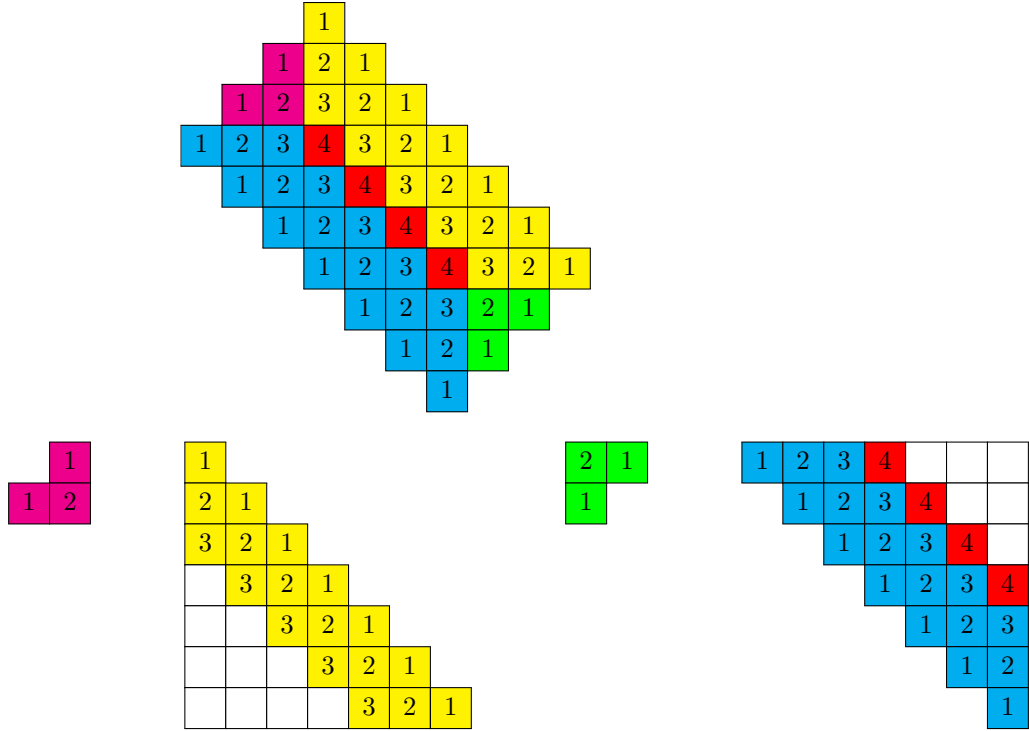


Figure 3.6: A square ice configuration of $\ell = 4$ decomposed into 4 plane partitions, except for the missing piece in white, which is negligible for $\ell \ll n^{1/3}$.

CHAPTER 4

Analytical Results

4.1 2D Oranges

Stepping the problem down by one dimension, one might ask the same question for the enumeration of stacks of oranges in 2 dimensions, as shown in Figure 4.1.

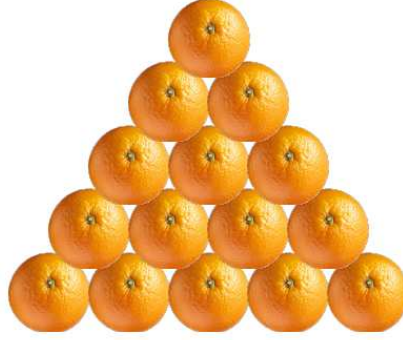


Figure 4.1: A stack of 2D oranges with $\ell = 1$.

It is seen (Figure 4.2) that for the case $\ell = 1$, the enumeration is the same as that of integer partitions. Also, for different values of ℓ , the pyramid is cut off at the top (Figure 4.3), and hence enumeration can be done as shifted partitions. It is possible to determine generating functions for some values of ℓ .

Let the enumeration of 2D orange stacks be denoted by $b_\ell(n)$. They can be enumerated by using the Bratley-McKay algorithm, in the same way as enumeration of integer partitions, except with the blocked blue region as initial condition. Such enumeration leads to the following results. For $\ell > 5$, there are no closed form representations of the sequences obtained.

- For $\ell = 1$, clearly $b_1(n) = p(n)$.
- For $\ell = 2$, $b_2(n) = p(n + 1)$, because the block at the origin can be considered as present by default, but not counted.
- For $\ell = 3$, $b_3(n) = p(n + 3) - 2$.
- For $\ell = 4$, $b_4(n + 6) = p(n + 6) - (n + 6) + 2 - 2p(n + 6|2 \text{ parts})$.

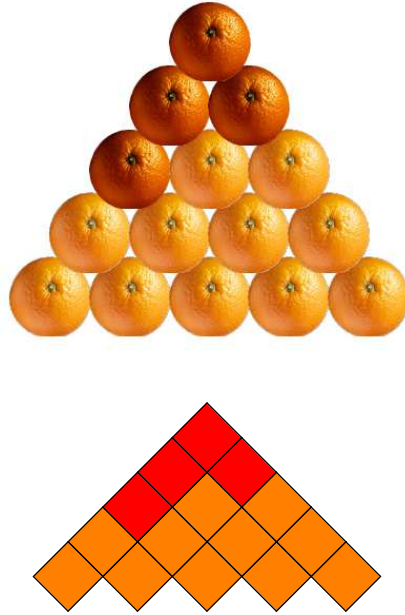


Figure 4.2: The red oranges represent the oranges that have been removed from the stack. Counting the number of ways of removing oranges from such a stack is clearly given by integer partitions, as can be seen from the second figure.

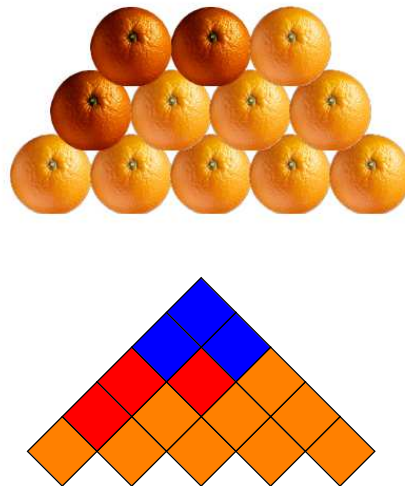


Figure 4.3: A stack of $\ell = 3$ with the corresponding partition representation. The blue part represents the missing portion, which results in the counting being given by shifted partitions.

4.2 Some results on partitions

4.2.1 Addition and Deletion Operators

Definition 4.1. Define the following operators on a general D dimensional partition λ

-

$$D = \sum_{i=1}^{N_-} D_i, U = \sum_{i=1}^{N_+} U_i,$$

where D_i and U_i are operators that indicate deletion and addition of a node at position i of λ respectively. N_+ and N_- are the number of positions in λ where a node may be added or deleted respectively.

Since the square ice resembles plane partitions far away from the origin, it is important to understand the action of these operators on partitions, to understand their behaviour on square ice.

Proposition 4.1. $DU - UD = (N_+ - N_-)I$.

Proof. For all pairs of nodes i, j such that addition or deletion of a node at one of them does not affect the addition or deletion at the other, the operators commute. That is, $D_i U_j - D_j U_i = 0$. Also, when the operations are performed on the same spot, $\sum_{i=1}^{N_-} \sum_{j=1}^{N_+} D_i U_j = N_+ I$ and $\sum_{i=1}^{N_+} \sum_{j=1}^{N_-} U_i D_j = N_- I$.

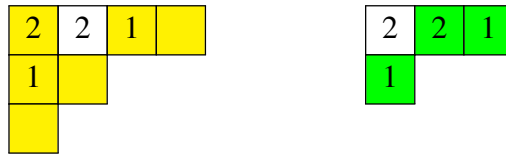


Figure 4.4: Here, the blue nodes belong to $S_+(\lambda)$ and the green nodes belong to $S_-(\lambda)$.

Let $S_{\pm}(\lambda)$ denote the set of nodes addable or removable from λ . Let λ' be the new partition obtained after an operation is performed, and b_i be the node on which the operation is performed. After U , $S_-(\lambda') = S_-(\lambda) + b_i +$ (local changes). After D , $S_+(\lambda') = S_+(\lambda) + b_i +$ (local changes). Clearly, when the commutation is performed, only the identity remains, leading to $(N_+ - N_-)I$. \square

Posets that satisfy $DU - UD = rI$, $r > 0$, for some r are called differential posets [15, 16]. The Young lattice is a poset with ordering such that, for 2 partitions $\lambda =$

$\{\lambda_1, \lambda_2, \dots\}$ and $\mu = \{\mu_1, \mu_2, \dots\}$ (λ_i and μ_i arranged in descending order here), $\lambda < \mu$ if and only if $\lambda_i < \mu_i$ for every i . Thus integer partitions are differential posets with $r = 1$.

Definition 4.2. Define $n_+^d(n)$ and $n_-^d(n)$ as the average number of additions and removals made over all partitions for a given n , i.e -

$$n_+^d(n) = p_d(n)^{-1} \sum_{i=1}^{p_d(n)} N_+(\lambda_i) \text{ and } n_-^d(n) = p_d(n)^{-1} \sum_{i=1}^{p_d(n)} N_-(\lambda_i).$$

Proposition 4.2. $n_{\pm}^d(n) \sim P_1 n^{d/d+1} + P_2^{\pm} n^{d-1/d+1} + P_3^{\pm}$.

Proof. The condition of detailed balance is given by

$$p_d(n) n_+^d(n) = p_d(n+1) n_-^d(n+1), \quad (4.1)$$

$$\therefore \log \frac{n_+^d(n)}{n_-^d(n+1)} = \log \frac{p_d(n+1)}{p_d(n)} \sim n^{-1/d+1}. \quad (4.2)$$

By observation of integer and plane partition data (Figure 4.5), it is clear that

$$n_+^1(n) - n_-^1(n) = 1 \text{ and } n_+^2(n) - n_-^2(n) \sim n^{1/3}.$$

Therefore, we might make the general assumption $n_+^d(n) - n_-^d(n) \sim n^{d-1/d+1}$.

This implies that $n_{\pm}^d(n) \sim P_1 n^{\alpha} + P_2^{\pm} n^{d-1/d+1} + P_3^{\pm}$. Substituting this expression in the detailed balance condition and solving to leading order yields $\alpha = \frac{d}{d+1}$. \square

From the observed data, and the form of $n_{\pm}(n)$, the following conjecture may be made.

Conjecture 4.1. $n_{\pm}^d(n+1) > n_{\pm}^d(n)$.

Proposition 4.3. In the asymptotic limit, $n_+^d(n) > n_-^d(n)$.

Proof. From the condition of detailed balance - $\frac{n_+^d(n)}{n_-^d(n+1)} = \frac{p_d(n+1)}{p_d(n)}$.

In the asymptotic limit, $\log p_d(n) \sim n^{d/d+1}$, which is an increasing function. Hence, $p_d(n+1) > p_d(n)$. This implies that $n_+^d(n) > n_-^d(n+1)$. From the Conjecture 4.1, $n_-^d(n+1) > n_-^d(n)$, which gives -

$$n_+^d(n) > n_-^d(n).$$

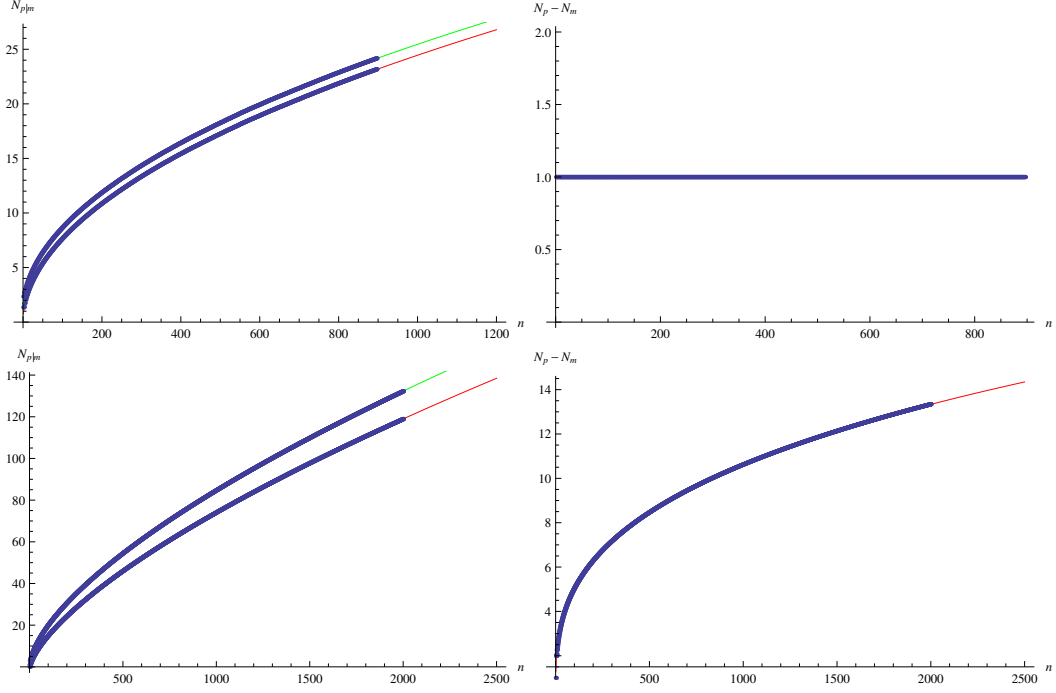


Figure 4.5: Plots for $n_+(n)$, $n_-(n)$ and their difference, for integer partitions(top) and plane partitions(bottom). The averages data (in blue) have been fit to the model described in Proposition 3. The fit for n_+ is in green and the fit for n_- is in red. The difference plot shows the leading behaviour is $n^{d-1/d+1}$, which in the case of integer partitions is a constant, viz. 1.

An analytic proof for $n_+^d(n) > n_-^d(n)$ for all integers is yet to be given. \square

4.3 Analytic form of $a_\ell(n)$

Despite the absence of a closed form expression for $a_\ell(n)$, we can still propose the form it takes for various ℓ given n , or vice versa. This leads to various expressions for $a_\ell(n)$, as described in this section.

Table 4.1 lists the exact enumeration of $a_\ell(n)$ for ℓ going from 1 to 6. The following conjecture for $a_\ell(n)$ was made by exact enumeration. $a_\ell(0)$ is set to 1.

Conjecture 4.2. *The expressions for $a_\ell(n)$ for different ℓ , given n , are -*

$$a_\ell(1) = \binom{\ell}{1}$$

$$a_\ell(2) = \binom{\ell}{2} + 4$$

$$a_\ell(3) = \binom{\ell}{3} + 6\ell, \ell \geq 2$$

$$a_\ell(4) = \binom{\ell}{4} + 8\binom{\ell}{2} - \ell + 23, \ell \geq 2$$

$\ell \backslash a(n)$	1	2	3	4	5	6
$a(0)$	1	1	1	1	1	1
$a(1)$	1	2	3	4	5	6
$a(2)$	4	5	7	10	14	19
$a(3)$	10	12	19	28	40	56
$a(4)$	24	29	44	68	103	152
$a(5)$	51	64	98	158	247	378
$a(6)$	109	139	213	350	567	898
$a(7)$	222	286	448	750	1252	2042
$a(8)$	452	582	918	1559	2668	4476
$a(9)$	890	1148	1832	3170	5539	9526
$a(10)$	1732	2227	3584	6292	11214	19740
$a(11)$	3298	4234	6882	12252	22247	39978
$a(12)$	6204	7950	13012	23445	43300	79342
$a(13)$	11470	14692	24220	44164	82871	154650
$a(14)$	20970	26842	44480	81995	156152	296489
$a(15)$	37842	48438	80678	150288	290202	560022
$a(16)$	67572	86509	144697	272150	532430	1043404
$a(17)$	119368	152902	256775	487388	965395	1919708
$a(18)$	208943	267783	451305	863887	1731351	3491081
$a(19)$	362389	464766	786008	1516592	3073660	6280514
$a(20)$	623438	800095	1357414	2638648	5404984	11185375
$a(21)$	1064061	1366512	2325540	4552488	9420512	19734004
$a(22)$	1802976	2316840	3954366	7792566	16282463	34509347
$a(23)$	3033711	3900502	6676369	13239698	27922063	59847208
$a(24)$	5071418	6523432	11196599	22336630	47527430	102976946
$a(25)$	8424788	10841282	18657454	37433466	80331385	175877782
$a(26)$	13913192	17909533	30901434	62337628	134873275	298279841
$a(27)$	22847028	29416966	50884452	103186612	225015223	502496682
$a(28)$	37315678	48055443	83327163	169824540	373141724	841161007
$a(29)$	60631940	78093926	135733071	277967860	615224276	1399559416
$a(30)$	98030644	126276743	219978688	452594316	1008792896	2315201903

Table 4.1: Explicit enumeration of $a_\ell(n)$ for $\ell = 1, \dots, 6$.

$$a_\ell(5) = \binom{\ell}{5} + 10\binom{\ell}{3} - 2\binom{\ell}{2} + 36\ell - 14, \ell \geq 3$$

$$a_\ell(6) = \binom{\ell}{6} + 12\binom{\ell}{4} - 3\binom{\ell}{3} + 53\binom{\ell}{2} - 25\ell + 132, \ell \geq 3$$

$$a_\ell(7) = \binom{\ell}{7} + 14\binom{\ell}{5} - 4\binom{\ell}{4} + 74\binom{\ell}{3} - 40\binom{\ell}{2} + 220\ell - 182, \ell \geq 4$$

$$a_\ell(8) = \binom{\ell}{8} + 16\binom{\ell}{6} - 5\binom{\ell}{5} + 99\binom{\ell}{4} - 59\binom{\ell}{3} + 345\binom{\ell}{2} - 308\ell + 858, \ell \geq 4$$

$$a_\ell(9) = \binom{\ell}{9} + 18\binom{\ell}{7} - 6\binom{\ell}{6} + 128\binom{\ell}{5} - 82\binom{\ell}{4} + 515\binom{\ell}{3} - 488\binom{\ell}{2} + 1463\ell - 1764, \ell \geq 5$$

Counting based explanations for these conjectures can be made for small values of n .

Since $a_\ell(n)$ refers to the number of ways of choosing n oranges from a stack of given

ℓ , an explicit enumeration leads to the following -

- $a_\ell(0) = 1$, fixed by choice.
- $a_\ell(1) = \binom{\ell}{1}$. - We pick one orange from the only available layer, which has ℓ oranges.
- For $a_\ell(2)$, the counting involves
 - $\binom{\ell}{2}$. (We pick both oranges from Layer 1)
 - $\binom{2}{1}\binom{2}{1} = 4$. (We pick one from Layer 1, one from the 2 exposed oranges in Layer 2, because of picking the first orange. Since we need the picking of the first orange to expose some oranges in the second layer, there are only two options for the first layer as well - the ones at the ends.)

$$\text{Sum} = \binom{\ell}{2} + 4.$$

- For $a_\ell(3)$, the counting involves
 - $\binom{\ell}{3}$. (We pick both oranges from Layer 1)
 - $\binom{4}{1} + \binom{2}{1}\binom{2}{1}\binom{\ell-3}{1} + \binom{2}{1}\binom{4}{1} + \binom{\ell-3}{1}\binom{2}{1}$. (There are many ways of picking two oranges from Layer 1 and one from Layer 2, each taking care of whether the oranges form the ends of Layer 1, or if they are consecutive, and how many oranges of the second layer they open up.)
 - $\binom{2}{1}$. (The only way of picking one orange from Layer 1 and two from Layer 2 is to pick one of the ends and follow it by picking both exposed oranges of Layer 2.)
 - $\binom{2}{1}\binom{2}{1} = 4$. (Similar to the previous choice, we pick one of the ends from Layer 1, one of the two exposed oranges from Layer 2, and further, the only exposed orange from Layer 3)

$$\text{Sum} = \binom{\ell}{3} + 6\ell.$$

This way of decomposing the final expression becomes highly non-trivial for higher n . Though this conjecture is based on exact enumeration, we are yet to understand the form that each expression takes. The alternating signs of the coefficients and the absence of the $\binom{\ell}{n-1}$ terms are especially noteworthy, and need to be explained, perhaps with the help of a new statistic.

4.3.1 Conjecture on generalized $a_\ell(n)$

Conjecture 4.3. For $\ell \geq \lfloor \frac{n}{2} \rfloor$, $a_\ell(n)$ is given by the following polynomial -

$$a_\ell(n) = \binom{\ell}{n} + 2n \binom{\ell}{n-2} - (n-3) \binom{\ell}{n-3} + (2n^2 - 5n + 11) \binom{\ell}{n-4} - (2n^2 - 11n + 19) \binom{\ell}{n-5} + \dots$$

4.4 Analytic bounds on $a_\ell(n)$

Theorem 4.1. For a given ℓ , $a_\ell(n-1) < a_\ell(n)$.

Proof. Define a removable one-part of a partition as follows - consider a configuration λ of volume n . If there exists $x > 0$ such that the reduced height $r(x+l-1, l-1) = 1$, and if setting this height to zero (removing a block, or equivalently, adding an orange at the node) leads to a valid configuration of volume $n-1$, then the node $(x+l-1, l-1)$ is called a removable one part. A given configuration might or might not have removable one parts, and there exists at least one configuration with no removable one-parts for every volume n , as demonstrated in the Figure 4.6.

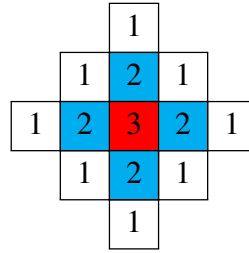


Figure 4.6: An example of a configuration with no removable one-part.

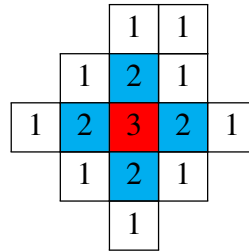


Figure 4.7: An example of a configuration with a removable one-part.

Reversing the statement, one can always add a removable one-part to a configuration of volume $n - 1$ to make a valid configuration of volume n . So each configuration of volume $n - 1$ corresponds uniquely to a configuration of volume n . Therefore

$$\boxed{a_\ell(n) = a_\ell(n - 1) + a_\ell(n | \text{no removable one parts}) > a_\ell(n - 1).} \quad (4.3)$$

□

4.4.1 Lower Bound for $a_\ell(n)$

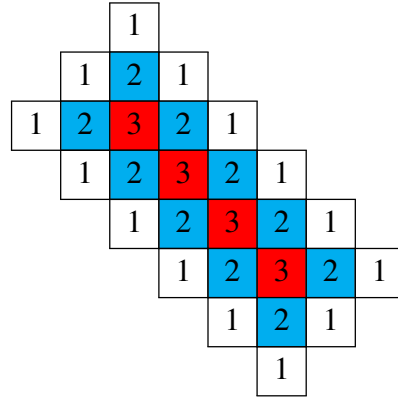


Figure 4.8: A configuration of $\ell = 4$ and $n = 46$.

Consider configurations like the one shown in Figure 4.8. For $m > 0$, the volume of such configurations is given by $n = \sum_{j=1}^{m+1} j(j + \ell - 1)$. Say we pick the first type. There are 2^{n_0} such configurations with columns ranging from n to $n - n_0$, where $n_0 = (m + 1)(m + \ell)$, the number of oranges in the $(m + 1)$ -th layer. Clearly,

$$\sum_{n=n_0}^n a_\ell(n) > 2^{n_0} \implies n_0 a_\ell(n) > 2^{n_0}.$$

Since $n_0 \sim (3n)^{2/3} - (3n)^{1/3} + O(1)$, and $m \sim (3n)^{1/3} - \frac{(l+2)}{2} + O(n^{-1/3})$, (under the conditions $n \rightarrow \infty, \ell \ll n^{1/3}$) we can put them together to get the bound on $\log a_\ell(n)$ as follows -

$$n_0 a_\ell(n) > 2^{n_0} \implies \log a_\ell(n) > n_0 \log 2 - \log n_0 > n_0 \log 2 = C_L n^{2/3} + O(n^{1/3}).$$

where $C_L = 3^{2/3} \log 2 = 1.4418$. Therefore,

$$\boxed{\log a_\ell(n) > 1.4418 n^{2/3}} \quad (4.4)$$

under the conditions $n \rightarrow \infty, \ell \ll n^{1/3}$.

4.4.2 Upper Bound on $a_\ell(n)$

As indicated before, the upper bound will be fixed by the observation that the square ice resembles plane partitions in the long range. Every configuration of square ice can be broken into 4 plane partitions/skewed plane partitions as shown in Figure 3.6.

If $p_2(n)$ indicates number of plane partitions of volume n , let $p_\ell(n)$ indicate number of skew plane partitions of the shape λ/μ_ℓ , where μ_ℓ is a plane partition that has ℓ parts, and a largest part ℓ , i.e., forms a right triangle of side ℓ at the origin. It can be seen that each configuration has 2 plane partitions and 2 such skew partitions. Therefore,

$$a_\ell(n) < \sum_{\sum n_i = n} \prod_{j=1}^2 p_2(n_j) \prod_{j=3}^4 p_\ell(n_j) < \sum_{\sum n_i = n} \prod_{j=1}^2 p_2(n_j) \prod_{j=3}^4 p_2(n_j + \frac{\ell^2}{2}(3n)^{1/3}).$$

This follows from the maximum ways of filling up the part μ_ℓ . Since $\ell \ll n^{1/3}$, this section becomes $O(1)$. Also, an upper bound can be fixed by maximizing the 4 plane partitions to be equal in volume. Therefore,

$$a_\ell(n) < p(n|4 \text{ parts}) p_2(\frac{n}{4})^4.$$

Since $p(n|4) \sim O(n^3)$ [17],

$$\boxed{\log a_\ell(n) < 4 \log p_2(\frac{n}{4}) \sim 3\zeta(3)^{1/3} n^{2/3} = 3.1898 n^{2/3}}, \quad (4.5)$$

using the asymptotic behaviour of $\log p_2(n)$ [10].

4.4.3 Final conjecture

Proposition 4.4. *Putting the above two results together, it is clear that*

$$\boxed{3^{2/3} \log 2 < n^{-2/3} \log a_\ell(n) < 3\zeta(3)^{1/3}.$$

Conjecture 4.4. *From the previous proposition, it can be seen that $n^{-2/3} \log a_\ell(n)$ tends to an ℓ -independent constant as $\rightarrow \infty$, and $\ell \ll n^{1/3}$.*

The heuristic explanation for this can be seen by examining large rectangles. As explained before, for $n \gg \ell^3$, the number of oranges in the rectangle go as $(3n)^{1/3}((3n)^{1/3} + \ell) \sim (3n)^{2/3} + O(\ell n^{1/3})$. Since $\ell \ll n^{1/3}$, the ℓ term is heavily suppressed, and does not feature in the counting when the asymptotic limit is considered. We further show that the estimates of the Monte Carlo simulations lie within these bounds.

CHAPTER 5

Simulation Methods

5.1 Monte Carlo simulations

Monte Carlo simulations, so named for city of the same name in France and its popular gambling culture, are one of the strongest tools to examine systems that are finite sized, and exist in a very large number of microstates. They provide a systematic means for determining ensemble averages of various measurables of the system by statistically visiting certain microstates, and using weighted averages to estimate the actual ensemble average. The system is setup as desired in a certain microstate of the system, chosen arbitrarily, or to create a specific bias, as the need may be. The system is then allowed to randomly pick microstates to jump to. The choice of states, weighting of these states and the statistical spread of the visited microstates form the basis of the algorithm.

Monte Carlo simulations are typically setup for Markovian processes [18]. So a transition rate can be used to enable the system to move between states. A steady state is obtained when the system attains detailed balance, that is, when the rate of outflow from a specific microstate equals the rate of inflow into the state. Such a condition is usually obtained when the distribution of states is uniform. When detailed balance is attained, the system is in steady state, and the required ensemble averages can be accurately calculated [19].

5.1.1 The Metropolis-Hastings Algorithm

The most popular type of Monte Carlo simulations is the Metropolis-Hastings Algorithm. The algorithm is implemented for canonical ensembles that are Markovian in nature, i.e. systems that can exchange energy with a temperature bath, but remain at the fixed temperature of the bath. Hence, the tunable parameter for these systems is the temperature of the bath. The boltzmann weight assigned to each state is given by

$e^{-\beta E}$, where E is the energy of the system in the current microstate, and β is the inverse temperature $\frac{1}{k_B T}$. Therefore, the partition function of such systems is given by

$$Z = \text{Tr}(e^{-\beta H}),$$

where H is the Hamiltonian of the system. It is clear that the system has a higher probability of existing in microstates of lower energies, and hence, would prefer to spontaneously jump from a state of higher energy to one with lower energy. The reverse process, while possible, would not be spontaneous.

The Metropolis algorithm exploits this fact to create a transition rate between states. Consider the system which is in the current state x , and proposes to jump to state x' . The condition of detailed balance is stated as -

$$P(x)P(x \rightarrow x') = P(x')P(x' \rightarrow x) \implies \frac{P(x \rightarrow x')}{P(x' \rightarrow x)} = \frac{P(x')}{P(x)} = e^{-\beta \Delta E}.$$

The ratio $\frac{P(x \rightarrow x')}{P(x' \rightarrow x)}$ is called the transition probability or the acceptance rate $W_{xx'}$. When $\Delta E = E_{x'} - E_x < 0$, the transition probability is greater than 1. So the transition takes place with full certainty, and the proposed state is accepted as the new state, as it has a lower energy as compared to the current state. If it is greater than one, then the higher energy state x' is accepted with probability equal to $e^{-\beta \Delta E}$. Therefore, the new state x' is accepted with a probability = $\text{Min}(1, e^{-\beta \Delta E})$.

This entire process of picking a proposed state and accepting or rejecting it is called one Monte Carlo step, and the process is repeated until the required distribution of states is obtained.

5.2 Transition Matrix Monte Carlo

The Transition Matrix Monte Carlo is used when transitions can only occur between "adjacent" microstates, and the transition probabilities depend on details of the 2 states involved. So a matrix can be populated with the transition probabilities between any 2 states. The problem of counting oranges can be cast into that of a transition matrix Monte Carlo algorithm.

The pyramid of peak length ℓ , and the shapes formed by removal of oranges from the pyramid is the structure of interest. By adding or removing oranges, each structure becomes part of a Bratelli diagram, where the addition and removal form the means of traversing the diagram through its edges. That is, each configuration leads to multiple other possible valid configurations connected through the edges of the diagram. Thus, all transitions occur between states that are adjacent on the Bratelli diagram. Traversing the diagram by probabilistic means and keeping track of the number ways to move out of a particular configuration forms the basis of the algorithm.

The system is Markovian in nature, since it has a finite system size, and hence a finite phase space that is covered by traversing its Bratelli diagram. The system is aperiodic, and hence is suitable for the implementation of Markovian Monte Carlo methods. Since the simulation is carried out stepwise, it is essentially a simulation of discrete-time Markov chains.

Consider a given configuration λ of n oranges. We define the following terms -

- $N_+^\ell(n)$ - The number of oranges that may be removed to the current configuration of oranges
- $N_-^\ell(n)$ - The number of oranges that may be added to the current configuration of oranges
- $n_+^\ell(n)$ - The number of oranges that may be removed to a configuration of n oranges, averaged over all possible configurations
- $n_-^\ell(n)$ - The number of oranges that may be added to a configuration of n oranges, averaged over all possible configurations
- $a_\ell(n)$ - The number of valid configurations for a given n .

The number of possible configurations, and possible positions of change grow very rapidly, as can be seen from the first few exactly calculated numbers. So to explicitly find $a_\ell(n)$ is a costly process, both in terms of time and resources. What might be more useful is to estimate the asymptotic behaviour of $a_\ell(n)$. Thus, in order to estimate the nature of the growth, we use an alternative method, by finding average number of additions and removals that are possible per n . We use Monte Carlo simulations to achieve this end.

Here, it may be noted that the algorithm establishes transition probabilities between configurations that are on adjacent rows of the Bratelli diagram. This can be visualized

as a matrix with transition probabilities on the primary off-diagonal both in the upper and lower triangles. The diagonal would thus have the forbidden transitions.

Probabilistically traversing the Bratelli diagram is essentially a method of sampling certain configurations of the system, as opposed to visiting every possible configuration. If weighted appropriately, sampling the configurations is sufficient to estimate ensemble averages of relevant quantities.

The algorithm is set up such that each Monte Carlo sweep takes the following steps [20, 21].

```
begin sweep

find possible_additions and possible_removals;
update counters with weight:
    1/{number(possible_additions)+number(possible_removals)};
Define prob_thermal=exp{-1/(temperature x scale)};
Choose chosen_pos uniformly from
    possible_additions and possible_removals;
According to chosen_pos,
    choose either to_add_orange or to_remove_orange;
If to_add_orange,
    Perform add_orange at chosen_pos;
Else if to_remove_orange,
    Perform remove_orange with probability prob_thermal;

end sweep.
```

Thus the Monte Carlo step is completed for the specific temperature. The temperature could be varied to get the required distribution. The sweep is performed over a range of temperatures from T_{\min} to T_{\max} , and a scale chosen by trial and error, to ensure a uniform distribution of hits over the range of n . When the Monte Carlo sweeps have been performed in repeated cycles of temperature sweeps, one can see that the system "thermalizes" in its distribution, i.e., it reaches a stationary probability. In terms of the

transition matrix W and the probability distribution vector Π , this is given as

$$W\Pi = \Pi. \quad (5.1)$$

The attainment of stationary probability also guarantees detailed balance, i.e, the rate of climbing up the Bratelli diagram equals the rate of climbing down. Satisfying detailed balance ensures uniform sampling distribution over the range of integers under consideration. Mathematically, this is expressed as -

$$a_\ell(n)n_+^\ell(n) = a_\ell(n+1)n_-^\ell(n+1). \quad (5.2)$$

Thus, the Monte Carlo sweeps are performed until stationary probability is reached. This could, in theory, be done until a pre-calculated "stopping time" is reached, which we do not perform here. Instead, we look at the nature of the obtained distribution, and compare the simulated ensemble averages with exactly calculated numbers to establish that the stationary probability distribution has been attained.

Once the stationary probability is reached, we now use the counter data to calculate the average quantities n_+^ℓ and n_-^ℓ . The calculated averages and the detailed balance condition, along with specified boundary conditions give the list of $a_\ell(n)$ when applied recursively in the following manner.

$$a_\ell(n) = a_\ell(0) \prod_{k=1}^n \frac{n_+^\ell(k-1)}{n_-^\ell(k)}. \quad (5.3)$$

The minimum and maximum temperatures, and the temperatures used were dependent on the specific run. The data was collected for 1000 oranges, 2000 oranges and 4000 oranges.

To sum up, we estimate $a_\ell(n)$ by using the Markovian nature of traversing the Bratelli diagram. We calculate the ensemble averages $n_\pm(n)$ and further use the averages to estimate $a_\ell(n)$. Error bars are established by comparing the obtained data with exactly calculated numbers available. Thus, the asymptotic behaviour is determined by a two-step process.

CHAPTER 6

Results

The method of employing Monte Carlo simulations to estimate the asymptotic behaviour has been elaborated before. Based on analytic bounds, it is conjectured that $a_\ell(n)$ will take the following form -

$$\log a_\ell(n) \sim \alpha_1 n^{2/3} + \alpha_2 n^{1/3} + \alpha_3 + g \log n.$$

From the condition of detailed balance $a_\ell(n-1)n_+(n-1) = a_\ell(n)n_-(n)$, it is clear that -

$$\log \frac{a_\ell(n)}{a_\ell(n-1)} = \log \frac{n_+(n-1)}{n_-(n)} \sim \frac{2}{3}\alpha_1 n^{-1/3} + \frac{1}{3}\alpha_2 n^{-2/3} + g n^{-1}.$$

So the required parameters to establish $a_\ell(n)$ can be found by fitting the ratio of n_+ and n_- instead. Since they are the actual quantities being determined by the simulation, this leads to greater accuracy in the asymptotics. It is also notable that the constant α_3 is absent in the above form.

6.1 Results of the simulation

The Monte Carlo simulation was run for values of n in the range [1,4200] for suitable number of iterations, and the data for $[\ell^3, 4200]$ was appropriately averaged before being fit to the above model to obtain the Table 6.1.

As can be seen from the data, α_1 is nearly ℓ -independent, while α_2 and g are clearly dependent on ℓ . The parameter α_1 can be estimated as 2.344 ± 0.002 .

If another term is added to the expression to make it

$$\log \frac{n_+(n-1)}{n_-(n)} \sim \frac{2}{3}\alpha_1 n^{-1/3} + \frac{1}{3}\alpha_2 n^{-2/3} + g n^{-1} + \epsilon n^{-4/3},$$

ℓ	α_1	α_2	g
1	2.34438	-0.0142642	-0.743792
2	2.34433	-0.0129182	-0.741693
3	2.34488	-0.0433843	-0.653471
4	2.34549	-0.0872087	-0.479429
5	2.34624	-0.14655	-0.209070
6	2.34662	-0.195253	0.121852

Table 6.1: Results of the three parameter fit.

then Table 6.2 is obtained. It can be seen that the estimate of α_1 still holds. This table indicates a possible suppression of the parameter α_2 . So after fitting with α_2 removed, we obtain Table 6.3.

ℓ	α_1	α_2	g	ϵ
1	2.34387	-0.00885166	-0.791637	0.0800653
2	2.34361	-0.0210338	-0.817617	0.142351
3	2.34418	-0.00770004	-0.742808	0.196249
4	2.34432	-0.0231988	-0.658148	0.454063
5	2.34544	-0.099351	-0.354031	0.415889
6	2.34502	-0.0944759	-0.214161	1.06672

Table 6.2: Results of the four parameter fit.

The ℓ -dependence of g is given by -

$$g_\ell = -0.692854 - 0.908691\ell + 0.0288371\ell^2.$$

The asymptotic behaviour clearly follows the analytic form

$$a_\ell(n) \sim A\mu^{n^{2/3}}n^g.$$

ℓ	α_1	g
1	2.34393	-0.757374
2	2.34393	-0.755175
3	2.34365	-0.705109
4	2.34317	-0.596929
5	2.34259	-0.428581
6	2.34203	-0.198032

Table 6.3: Results of the two parameter fit.

When fit explicitly to this form as $\log a_\ell(n) \sim an^{2/3} + b \log n + c$, we can estimate μ and A . The parameters thus obtained are given in Table 6.4. The data estimates a as 2.343 ± 0.001 , which lies within the range predicted by the first fit. Fitting the $\log A$ term c gives -

$$\log A_\ell = -1.87944 + 0.257933\ell.$$

ℓ	a	b	c
1	2.34386	-0.750724	-1.68906
2	2.34389	-0.750636	-1.4316
3	2.3436	-0.70123	-1.03514
4	2.34297	-0.584432	-0.690943
5	2.34213	-0.39474	-0.50498
6	2.34131	-0.13896	-0.508337

Table 6.4: Fit to analytic form to estimate A_ℓ .

6.2 Summary of results

In conclusion, the results obtained during the course of this project are summarized below.

- The square ice was modelled in the form of stacking oranges, and the first few numbers of the sequence were explicitly enumerated by appropriately modifying the Bratley-McKay algorithm [22].
- Conjecture 4.3, on the analytic form of the sequence $a_\ell(n)$, was derived from the generated data, for a given ℓ , for $n = 1$ to 9.
- Conjecture 4.3, on the analytic form of the sequence $a_\ell(n)$, was derived from the generated data, for a given n .
- A Monte Carlo code was developed to calculate the required averages n_+ and n_- numerically. The generated data was fit to appropriate models, and the required coefficients were obtained. Three such parameter fits were executed.
- It was observed that the simulated data agreed with the exactly calculated numbers, and the three fits overlap in the region $n \gg \ell^3$, where the asymptotic behaviour holds.
- Bounds on the asymptotic behaviour of $a_\ell(n)$ were analytically established, and a conjecture (Conjecture 4.4) was proposed regarding its limit value.

- The numerical simulations were shown to lie between the theoretically established bounds $\ell \ll n^{1/3}$, $1.4418 < n^{-2/3} \log a_\ell(n) < 3.1898$.
- Conjecture 4.5, which stated that $n^{-2/3} \log a_\ell(n) \rightarrow C$, for large n , was also established. The ℓ -independent constant was determined to be $C = 2.344 \pm 0.002$.
- The four-parameter model gives the significant ℓ -dependent parameter $g_\ell = -0.692854 - 0.908691\ell + 0.0288371\ell^2$.
- The data was also fit to the analytic form $a_\ell(n) \sim A\mu^{n^{2/3}}n^g$. The ℓ -dependence is given by $\log A_\ell = -1.87944 + 0.257933\ell$.

$n \backslash \ell$	1	2	3	4	5	6
1	4.	3.	3.33333	4.	4.8	5.66667
2	4.	3.6	4.42857	5.	5.57143	6.21053
3	4.4	4.5	4.73684	5.35714	6.05	6.75
4	4.66667	4.96552	5.22727	5.88235	6.49515	7.14474
5	5.11765	5.5	5.77551	6.3038	6.94737	7.60318
6	5.46789	5.84173	6.22066	6.72	7.36332	8.00891
7	5.96396	6.26573	6.64955	7.12533	7.74042	8.39373
8	6.34513	6.5945	7.01852	7.5279	8.12331	8.77301
9	6.76854	6.94948	7.38264	7.89022	8.48059	9.12954
10	7.12933	7.27436	7.72628	8.24317	8.8361	9.4766
11	7.49545	7.61644	8.06117	8.58031	9.1736	9.8135
12	7.81883	7.9366	8.3765	8.90493	9.50095	10.1415
13	8.14612	8.26382	8.68592	9.21855	9.81632	10.4589
14	8.44864	8.57619	8.98595	9.52451	10.1246	10.7685
15	8.74732	8.88604	9.28026	9.82073	10.4235	11.0696
16	9.03321	9.18483	9.56815	10.1099	10.7154	11.3636
17	9.31608	9.47848	9.85231	10.3921	11.0002	11.6509
18	9.59022	9.76273	10.131	10.6682	11.279	11.9321
19	9.86206	10.0416	10.4055	10.939	11.5519	12.2074
20	10.1283	10.3128	10.6752	11.2051	11.8196	12.4775

Table 6.5: Data for $n_+(n)$, evaluated exactly by the Bratley-McKay algorithm.

$n \backslash \ell$	1	2	3	4	5	6
1	1.000000	1.000000	1.000000	1.000000	1.000000	1.000000
2	1.000000	1.200000	1.428571	1.600000	1.714286	1.78947
3	1.600000	1.500000	1.631579	1.785714	1.950000	2.10714
4	1.833333	1.862069	2.045455	2.205882	2.349514	2.48684
5	2.196079	2.250000	2.346939	2.531646	2.708502	2.87302
6	2.394495	2.532374	2.657277	2.845714	3.026455	3.20045
7	2.684685	2.839161	2.957589	3.136000	3.334665	3.52204
8	2.929204	3.079038	3.245098	3.427838	3.632309	3.82931
9	3.222472	3.343206	3.516921	3.702208	3.912800	4.12219
10	3.478060	3.582398	3.773716	3.975207	4.188871	4.40567
11	3.744087	3.826169	4.023685	4.233268	4.453994	4.67927
12	3.984526	4.056352	4.263526	4.483941	4.713279	4.94472
13	4.229119	4.294582	4.500206	4.727289	4.964233	5.20304
14	4.455698	4.523210	4.729609	4.965278	5.209590	5.4554
15	4.681782	4.752508	4.954201	5.196436	5.447833	5.70111
16	4.898715	4.975459	5.174351	5.423252	5.681336	5.94135
17	5.113531	5.196597	5.391810	5.645207	5.909697	6.17639
18	5.322227	5.412136	5.605582	5.863015	6.133674	6.4067
19	5.529442	5.624968	5.816928	6.076886	6.353322	6.63255
20	5.732570	5.833040	6.025264	6.287327	6.569233	6.85436

Table 6.6: Data for $n_-(n)$, evaluated exactly by the Bratley-McKay algorithm.

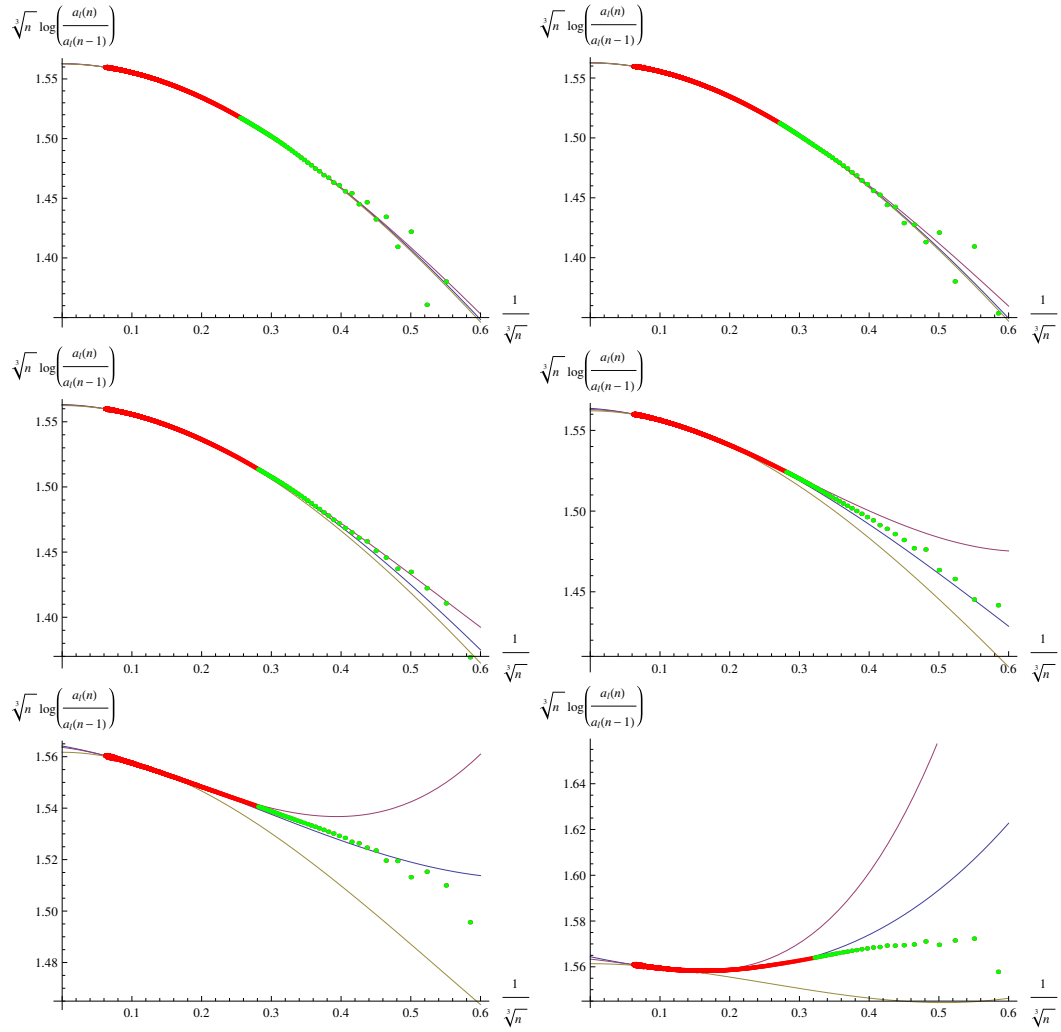


Figure 6.1: Plots of $\log \frac{a_\ell(n-1)}{a_\ell(n)}$ versus $n^{-1/3}$. The three fits, along with actual data and simulation data. The green points indicate explicitly enumerated data, the red points are the data generated in simulation. The pink line is the three parameter fit, the brown line is the three parameter fit, and the blue line is the four parameter fit. Note that they all agree for $n^{-1/3} \ll \ell^{-1}$. The plots represent data from $\ell = 1, \dots, 6$. Key: Black plot - Two parameter fit, Blue plot - Three parameter fit, Purple plot - Four parameter fit, Red points - Simulated data, Green points - Actual data

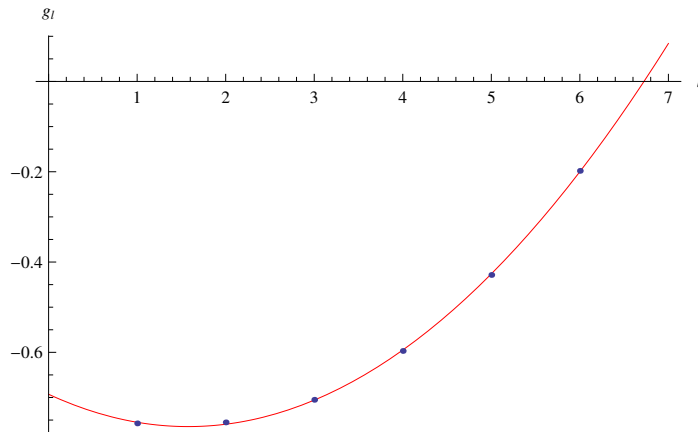


Figure 6.2: A fit of g as a function of ℓ .

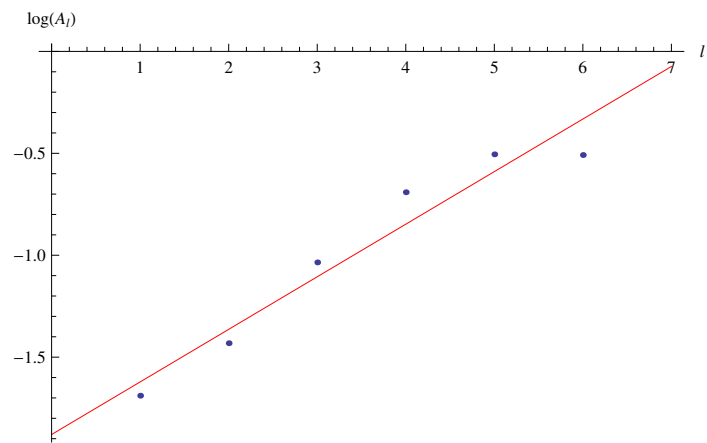


Figure 6.3: A fit of $\log A_\ell$ as a function of ℓ .

CHAPTER 7

Conclusion and Unresolved Issues

The primary question proposed in this thesis was to study the behaviour of $a_\ell(n)$ by decomposing it into plane partitions, and establish an exponent for its asymptotic behaviour. This question, along with an analytic study of the problem has been presented in this thesis so far. However, there are several unresolved questions with respect to the problem, some of which have been listed here.

- It can be seen from the generated data that the relation $a_\ell(n) > a_{\ell-1}(n)$ holds for ℓ between 1 and 6. It is conjectured that this relationship is true for all ℓ and a given n . However, this conjecture has yet to be analytically proven.
- There is no closed form representation of $a_\ell(n)$, but for a given ℓ , an expression for $a_\ell(n)$ for different n has been conjectured. This needs to be proved.
- Conjectures for $a_\ell(n)$, given n , have been made. They need to be further understood in terms of combinatorics, and a new statistic has to be found.
- It is possible that the operators D and U have an underlying algebra to them, with respect to generalized d -dimensional partitions, since these operations on other similar objects are known to have an associated algebra.
- The generated data shows that $n_+(n) > n_-(n)$ for n in the range $[1, 4200]$. The conjecture that this is true for all integers has to be established. It is easily shown in case of integer partitions though the proof has to be generalized for all dimensions.
- It is also seen that the averages $n_\pm(n+1) > n_\pm(n)$. This can be easily proved if the previous conjecture, when established, is used along with the condition of detailed balance.

Thus, there are several loose ends that have been left untied at the time of completion of this report, which will hopefully be resolved soon.

APPENDIX A

The Bratley-McKay Algorithm

The Bratley-McKay algorithm [22] is a method of explicitly counting multi-dimensional partitions. It can be modified as required to count configurations of any object that can be placed on a Bratelli diagram, including generalized square ice. The original partition algorithm is explained here.

Recall the following definition of an integer partition.

Definition A.1. *A partition λ of integer n can be defined as a collection of nodes such that if $(x_1, y_1) \in \lambda$, then $(x_2, y_2) \in \lambda$, $\forall x_2 \leq x_1$ and $y_2 \leq y_1$. The total number of nodes is n , and is also called the volume of the partition.*

This can be generalized to higher dimensions as -

Definition A.2. *A partition λ of integer n can be defined as a collection of nodes such that if $\{x_i\} \in \lambda$, then $\{y_i\} \in \lambda$, $\forall x_i \leq y_i$, $1 \leq i \leq d + 1$, where d is the dimension of the partition. The total number of nodes is n , and is also called the volume of the partition.*

Therefore, to get a new valid configuration of volume $n + 1$, a node has to be added such that it does not violate the condition described in the definition. But it should be noted that there are multiple such valid configurations that can be attained by adding a node at the appropriate position. The algorithm has to visit each configuration exactly once in order to count the total number of partitions of a given volume. This is done through a recursive algorithm. The algorithm is explained for integer partitions, and can be easily extended to higher dimensions as well.

We start with a node at the origin $(0, 0)$, which will be the only node in the current partition P . There are two possible locations to add nodes to get valid configurations, as per the required condition - $(0, 1)$ and $(1, 0)$. They are stored in the set of possible additions Poss_Add .

The central part of the algorithm is the recursive method that visits a partition, adds a node, updates Poss_Add and blocks certain nodes from being added, to avoid overcounting. Let it be called `addpart(n,from,to)`, where n is the number of nodes currently in P, and from and to determine which nodes are allowed, and which are blocked. Therefore, in the beginning, this routine will be called as `addpart(1,0,1)`, since there is 1 node in P and 2 possible nodes to be added. The routine would then go into recursion as described in the following pseudocode -

```

routine addpart (n, from, to)
for i=from; i=to; i++
{
addnode Poss_Add[i] to P;
if size of P=N, continue to end of loop;
update Poss_Add by adding "s" new nodes;
increment "to" by the number of nodes added to Poss\_Add;
addpart (n+1, i, to+s);
}

```

Here, N is the number whose integer partitions are to be enumerated. Note that we are adding the next node with the from adjusted to avoid overcounting. The only difference in enumerating higher dimensional partitions would be in the dimensionality of the nodes, and the complexity in checking for the condition while updating Poss_Add.

The algorithm can be used to enumerate any object with a Bratelli lattice structure. Given the condition for valid configurations, one can traverse the lattice and counting configurations after blocking nodes that would result in overcounting.

REFERENCES

- [1] *Online Encyclopedia of Integer Sequences*. <http://www.oeis.org>.
- [2] Demian Levis. *Two-dimensional Spin Ice the Sixteen-Vertex Model*. PhD thesis, Pierre and Marie Curie University, 2012.
- [3] L. Pauling. The structure and entropy of ice and of other crystals with some randomness of atomic arrangement. *Journal of the American Chemical Society*, 57(12):2680–2684, 1935.
- [4] Elliott H. Lieb. Residual entropy of square ice. *St. Petersburg Math. J.*, 21:407–421, 2010.
- [5] Greg Kuperberg. Another proof of the alternating sign matrix conjecture. *Internat. Math. Res. Notices*, 1996(3):139–150, 1996.
- [6] David Bressoud. *Proofs and Confirmations: The Story of the Alternating-Sign Matrix Conjecture*. Cambridge Univ. Press, 1999.
- [7] G. Andrews. Plane partitions V: The T.S.S.C.P. conjecture. *J. Combin. Theory Ser. A*, 66:28–39, 1994.
- [8] Jason Fulman. Stein’s method and plancherel measure of the symmetric group. *Trans. AMS.*, 2003.
- [9] P. A. MacMahon. Memoir on the theory of the partition of numbers. part I. *Philosophical Transactions of the Royal Society of London, Series A* 187, pages 619–673, 1896.
- [10] E. M. Wright. Asymptotic partition formulae I. plane partitions. *The Quarterly Journal of Mathematics* 1, pages 177–189, 1931.
- [11] D. P. Bhatia, M. A. Prasad, and D. Arora. Asymptotic results for the number of multidimensional partitions of an integer and directed compact lattice animals. *Journal of Physics A: Mathematical and General*, 30, 1997.

- [12] Benjamin Young. Computing a pyramid partition generating function with dimer shuffling. *Journal of Combinatorial Theory Series A*, 116.2:334–350.
- [13] Balazs Szendroi. Non-commutative donaldson-thomas theory and the conifold. *Geom.Topol.*, 12:334–350, 2007.
- [14] N. M. Bogolyubov. Five-vertex model with fixed boundary conditions. *Physical Review*, 162, 1967.
- [15] R. Stanley. Variations on differential posets, in invariant theory and tableaux. *IMA Vol. Math. Appl. 19, Springer, New York*, pages 145–165, 1990.
- [16] R. Stanley. Differential posets. *Journal of the American Mathematical Society*, 1(4), 1988.
- [17] G. E. Andrews and K. Eriksson. *Integer Partitions*. Cambridge Univ. Press, 2004.
- [18] Volker Schmidt. *Markov Chains and Monte-Carlo Simulation - Lecture Notes*. 2010.
- [19] K.P.N. Murthy. *Monte Carlo Methods in Statistical Physics*. Universities Press, 2004.
- [20] M. Widom, R. Mosseri, N. Destainville, and F. Bailly. Arctic octahedron in three-dimensional rhombus tilings and related integer solid partitions. *Journal of Statistical Physics*, 109:516, 2002.
- [21] Nicolas Destainville and Suresh Govindarajan. Estimating the asymptotics of solid partitions. *Journal of Statistical Physics*, 158:950, 2015.
- [22] P. Bratley and J. McKay. Algorithm 313: Multi-dimensional partition generator. *Communications of the ACM*, 10:666, 1967.

LIST OF PAPERS BASED ON THESIS

1. Suresh Govindarajan, Anthony J. Guttmann and Varsha Subramanyan On a square-ice analog of plane partitions. (Writing in progress.)